Acta Cryst. (1985). B41, 173-179

The Structural Location and Role of Mn^{2+} Partially Substituted for Ca^{2+} in Fluorapatite

BY P. R. SUITCH

School of Physics, Georgia Institute of Technology, Atlanta, Georgia 30332, *USA*

J. L. LACOUT

Laboratoire de Physico-Chimie des Solides, 38 *rue des Ponts, UA CNRS* 445, 31400 *Toulouse, France*

A. HEWAT

Institut Laue-Langevin, BP 156*X*, 30842 *Grenoble CEDEX, France*

AND R. A. YOUNG

School of Physics, Georgia Institute of Technology, Atlanta, Georgia 30332, *USA*

(*Received* 31 *July* 1984; *accepted* 21 *November* 1984)

Abstract

Mn substituting at the $\sim\frac{3}{8}$ atom-per-unit-cell level for Ca in fluorapatite, $Ca_{10}(PO_4)_6F_2$, goes essentially exclusively to a subset of the Ca(1) sites, Ca(1*a*) at $\frac{1}{3}, \frac{2}{3}, z (z \approx 0)$, thus lowering the crystal symmetry from $P6_3/m$ at least to $P6_3$ and perhaps to $P3$. No evidence was found for any Mn substituting as Mn^{5+}. One Mn in a Ca(1) site interacts with all six PO_4 groups in the unit cell, rotating them slightly and perturbing their ν_1 IR vibration from 968 to 959 cm^{-1}. Thus, the absorbance ratio $A(959)/[(A959)+(A968)]$ is directly the fraction of a Mn^{2+} ion per cell. The slight rotation explains the structure's tendency to resist accepting more than one Mn^{2+} per cell; that would call for some counter rotations. To avoid any counter rotations, even the one Mn^{2+} ion cell would have to occur in an ordered subset of the Ca(1*a*) sites. Interatomic distances obtained from results of refinements in $P3$ gave some evidence that this further ordering was already occurring to some degree in this specimen. The structure studies were carried out with Rietveld refinements with 5 K and room-temperature fixed-energy neutron powder-diffraction data. CaF_2 present as a minor impurity phase served well as an internal standard; refinement was carried out for both phases simultaneously.

Introduction

Manganese occurs naturally as a trace element in human dental enamel at the 0-7 p.p.m. level, where it has been implicated in cariogenesis (Curzon & Crocker, 1978), and in phosphate ores (*e.g.* 30 p.p.m., LaCout, 1983). Because phosphate ores are processed in such large quantities each year, they represent a potentially important source of Mn in spite of its low concentration. Mn substitution is important in the fluorescent-lighting industry because it can be introduced into synthetic fluorapatite, $Ca_{10}(PO_4)_6F_2$, both as Mn^{5+} substituting for P^{5+}, *i.e.* MnO_4^{3-} for PO_4^{3-} (Kingsley, Prener & Segall, 1965), and as Mn^{2+} substituting for Ca^{2+} (*e.g.* Ohkubo, 1969). Electron paramagnetic resonance, thermoluminescence (Kasai, 1962) and other studies (Johnson, 1962; Heughebaert, Seriot, Joukoff, Gaumemahn & Montel, 1975; Baratali, Heughebaert, Seriot & Montel, 1976) of single crystals of fluorapatite with trace amounts of Mn^{2+} have led to the conclusion that the Mn^{2+} was substituting for Ca^{2+} at the crystallographic site of Ca(1) and not at that of Ca(2), whereas other EPR studies have placed it in both sites, though primarily in the Ca(1) site (*e.g.* Gilinskaya & Shcherbakova, 1971; Warren, 1970; Warren & Mazelsky, 1974). For a description of the fluorapatite (FAp) crystal structure see, for example, Sudarsanan, Mackie & Young (1972).

Primarily from comparison of infrared spectra, LaCout (1983) concluded that the Mn^{2+} also substitutes preferentially, perhaps exclusively, at the Ca(1) site in powdered synthetic samples with much higher Mn contents, up to one Mn^{2+} ion per unit cell. He based this conclusion primarily on the occurrence of an additional phosphate ν_1 band in the IR spectrum at about 10 cm^{-1} lower frequency than the ν_1 band of phosphate unperturbed by Mn. This Mn-associated band increased regularly with increasing Mn content, as is shown in Fig. 1, until, at one Mn^{2+} ion per cell, only the Mn-perturbed ν_1 band was present. LaCout also found that (i) it was not possible to prepare (Ca, Mn)FAp with more than one Mn per unit cell with high-temperature methods and (ii) (Ca, Mn)FAp prepared in aqueous milieu (coprecipitation) with more than one Mn per cell decomposed on heating to, apparently, $Ca_9Mn_1(PO_4)_6F_2$ and various non-apatitic fluoridated phases.

0108-7681/85/030173-07$01.50

The present work was undertaken to determine the precise structural location and crystal-structural consequences of the substitution of Mn^{2+} into $Ca_{10}(PO_4)_6F_2$. Both equality of the absorbances of the two ν_1 bands with $\frac{1}{2}$ Mn per cell and the resistance of the structure to accommodation of more than one Mn per cell are explained by the present results.

Experimental

The off-white powder specimen was prepared by a double-decomposition method in an aqueous medium. A 0·1 *M* solution of calcium and manganese nitrate was poured slowly into a boiling solution of 0·06 *M* ammonium phosphate and ammonium fluoride. The precipitate was then calcined at 1173 K for 2 h in vacuum. The reactants were chosen in proportions to yield a product approximating $Ca_{9.5}Mn_{0.5}(PO_4)_6F_2$. The Mn content found in the product with wet chemical analysis was 0·448 atoms per unit cell. A small amount (<1 wt % by diffraction analysis) of CaF_2 occurred as a second phase in the product and was useful as an internal reference material. Other samples similarly prepared but with different Mn contents had been previously used by LaCout (1983) for collection of the IR spectra shown in Fig. 1; a Perkin-Elmer 457 infrared spectrometer operating in the transmission mode was used. That set of specimens and their IR spectra have been discussed by LaCout (1983).

Although the scattering factors of Ca and Mn are rather similar for X-rays, they are very different for thermal neutrons (4·9 and −3·6 fm, respectively). Therefore, the present crystal-structural analyses have been based on neutron diffraction data collected with unit *D1A* at Institut Laue-Langevin, Grenoble, with a fixed wavelength (~1·909 Å) and specimen temperatures of both 5 K and room temperature.

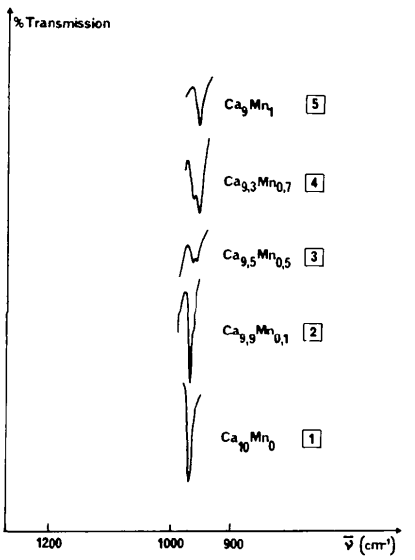

Fig. 1. Mn-perturbed (959 cm^{-1}) and unperturbed (968 cm^{-1}) ν_1 IR bands of the PO_4 group (from LaCout, 1983).

Structure refinement procedure and results

Rietveld-method crystal structure refinements from the neutron powder diffraction data were carried out with a slightly updated version, *DBW* 3.2, of the computer program described by Wiles & Young (1981). Pseudo-Voigt profile functions were used and background parameters were refined. Structural parameters in the CaF_2 phase were refined simultaneously with those in the apatite phase. Manganese was not put into the model; its presence and location can be inferred from the lowering of the apparent site-occupancy factors, *N*, for Ca at the site(s) where it substitutes. $N = p[xb_{Mn} + (1-x)b_{Ca}]/b_{Ca}$ where p is the multiplicity of the site, x is the fraction of the sites filled by Mn, b_{Mn} and b_{Ca} are the scattering lengths, and it is assumed that every Ca site is occupied by either Ca or Mn. The site occupancy for site O(3*a*) was kept fixed so that the overall scale factor could be varied conveniently.

Refinements for the apatite carried out in space groups $P6_3/m$, $P6_3$, and $P3$ demonstrated that the symmetry was lower than $P6_3/m$. Refinements in $P6_3$ with all anisotropic thermal parameters proceeded well (94 parameters) but led to some non-positive-definite thermal ellipsoids, as did refinements in $P3$ with individual isotropic thermal factors (97 parameters refined). Final refinements were, therefore, done in $P6_3$ with isotropic thermal parameters for most of the atoms and anisotropic for the three atoms that had exhibited the largest isotropic thermal parameters in earlier refinements.

The various numerical refinement indicators and refined parameter results for the final refinements in $P6_3$ appear in Table 1 along with Sudarsanan, Mackie & Young's (1972) results for fluorapatite. Similar results for the atomic coordinates were obtained both with all isotropic and with the mixed set of isotropic and anisotropic thermal factors. (The latter are shown in Table 1.) Fig. 2 shows the overall fit of the calculated to the observed diffraction pattern for both the apatite and the fluorite phases (combined) with the 5 K data. A similar fit was obtained with the room-temperature data. Fig. 2 and the values of the *R* factors in Table 1 show that good pattern-fitting was obtained. The facts that the site occupancy in CaF_2 refined to the stoichiometric value and that the individual isotropic thermal parameters refined to zero, within the precision expected, for the 5 K CaF_2 case attest to the probable accuracy of the apatite refinements.

The standard deviations for the refined parameters in Table 1 are agreeably small in view of the number of parameters refined (68). Obviously, the well crys-

Table 1. *Positional parameters and thermal parameters*

(*a*) Parameters from the refinements in $P6_3$ for (Ca, Mn) apatite compared to those of fluorapatite in $P6_3/m$

	Crystal*	*x*	*y*	*z*	*N*	B(Å^2)
	5K	0·3269 (2)	0·4853 (2)	0·2393 (13)	6·33 (12)	0·53 (4)
O(1)	RT	0·3272 (2)	0·4856 (2)	0·2418 (14)	6·29 (12)	0·94 (4)
	FAp	0·3262 (1)	0·4843 (1)	0·2500	6·00 (4)	0·65 (5)‡
	5K	0·5887 (1)	0·4685 (2)	0·2541 (14)	6·16 (12)	0·58 (5)
O(2)	RT	0·5878 (2)	0·4655 (2)	0·2611 (15)	6·29 (13)	1·12 (5)
	FAp	0·5880 (1)	0·4668 (1)	0·2500	6·00 (4)	0·74 (3)‡
	5K	0·3453 (7)	0·2607 (7)	0·0632 (11)	6·00 [22]†	0·34 (14)
O(3*a*)	RT	0·3450 (6)	0·2598 (8)	0·0670 (13)	6·00 [23]†	0·67 (13)
	FAp	0·3416 (1)	0·2568 (1)	0·0704 (1)	5·99 (2)	0·75 (4)‡
	5K	−0·3348 (8)	−0·2503 (6)	−0·0763 (12)	6.76 (24)	0·6 (6)‡
O(3*b*)	RT	−0·3332 (8)	−0·2521 (8)	−0·0746 (14)	6·78 (25)	1·6 (3)‡
	FAp	−0·3416	−0·2568	−0·0704	5·99	0·75‡
	5K	0·3990 (2)	0·3696 (2)	0·2366 (11)	5·98 (12)	0·03 (4)
P	RT	0·3986 (2)	0·3699 (2)	0·2402 (13)	5·94 (12)	0·24 (4)
	FAp	0·3981 (0)	0·3688 (0)	0·2500	5·95 (1)	0·33 (0)‡
	5K	0·3333	0·6667	−0·0023 (24)	1·40 (8)	0·26 (39)
Ca(1*a*)	RT	0·3333	0·6667	−0·0015 (21)	1·34 (7)	0·13 (37)
	FAp	0·3333	0·6667	0·0011 (0)	1·95 (1)	0·62 (0)‡
	5K	0·6667	0·3333	−0·0016 (18)	2·17 (7)	0·8 (6)‡
Ca(1*b*)	RT	0·6667	0·3333	−0·0005 (17)	2·23 (7)	1·7 (3)‡
	FAp	0·6667	0·3333	−0·0011	1·95	0·62‡
	5K	0·2415 (2)	−0·0072 (2)	0·2500	6·00 (11)	0·26 (5)
Ca(2)	RT	0·2408 (2)	−0·0077 (3)	0·2500	5·93 (11)	0·63 (5)
	FAp	0·2416 (0)	0·0071 (0)	0·2500	5·86 (1)	0·51 (0)‡
	5K	0·0000	0·0000	0·2458 (24)	2·09 (4)	1·1 (1)‡
F	RT	0·0000	0·0000	0·2463 (25)	2·09 (4)	1·9 (1)‡
	FAp	0·0000	0·0000	0·2500	1·88 (1)	1·03 (6)‡

(*b*) Anisotropic temperature factors for O(3*b*), Ca(1*b*) and F

	Crystal*	β_{11}	β_{22}	β_{33}	β_{12}	β_{13}	β_{23}
O(3*b*)	5K	0·0097 (8)	0·0016 (6)	0·0068 (8)	0·0037 (4)	−0·0008 (4)	−0·0005 (3)
	RT	0·0168 (9)	0·0053 (6)	0·0089 (8)	0·0078 (5)	−0·0036 (4)	−0·0016 (3)
Ca(1*b*)	5K	0·0033 (10)	0·0033 (10)	0·0037 (17)	0·0016 (5)	0	0
	RT	0·0074 (11)	0·0074 (11)	0·0067 (16)	0·0037 (6)	0	0
F	5K	0·0036 (3)	0·0036 (3)	0·0080 (7)	0·0018 (1)	0	0
	RT	0·0054 (3)	0·0054 (3)	0·0188 (8)	0·0027 (2)	0	0

R_{wp} = 4·37%, R_B = 1·17%, R_{exp} = 5·17%,§ and a = 9·3514 (1) and c = 6·8537 (1) Å at room temperature on the assumption that $a(CaF_2)$ = 5·4626 Å (Swanson & Tatge, 1951). Similarly, the values for 5 K were R_{wp} = 4·14%, R_B = 0·99%, R_{exp} = 5·17%, a = 9·3323 (1), c = 6·8424 (1) Å and a for CaF_2 = 5·4456 (1) Å.

For the CaF_2 phase at 5 K, B(Ca) = −0·25 (15), B(F) = 0·36 (9) Å^2, and N(Ca) = 0·95 (2) with N(F) fixed at unity. N is the site occupancy.

* 5 K and RT refer to the present specimen at 5 K and room temperature, respectively. FAp refers to synthetic fluorapatite as reported by Sudarsanan, Mackie & Young (1972).

† Site occupancy not varied; the [e.s.d.] is taken from the overall scale factor.

‡ These values are equivalent isotropic B's, where $B_{eq} = (8/3)\pi(u_{11} + u_{22} + u_{33})$ as calculated with *ORFFE*4 (Busing *et al.*, 1979) from Table 1(*b*) and the values reported by Sudarsanan, Mackie & Young (1972) for FAp.

§ $R_{wp} = \{\sum_i w_i[y_i(o) - y_i(c)]^2 / \sum_i w_i[y_i(o)]^2\}^{1/2}$ [in Wiles & Young (1981) the 1/2 was inadvertently omitted]. $R_B = \sum_K |'I_K(o)' - I_K(c)| / \sum_K 'I_K(o)'$ (see Wiles & Young, 1981). $R_{exp} = \{(N - P + C)/\sum w_i[y_i(o)^2]\}^{1/2}$ (R expected if the only errors were counting statistics), where $y_i(o)$ and $y_i(c)$ are the observed and calculated intensities at the ith step in the powder pattern, w_i is the weight, N is the number of observations, P is the number of parameters varied, and C is the number of constraints.

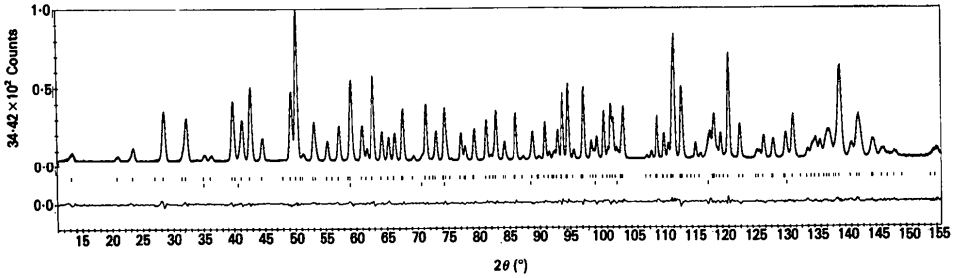

Fig. 2. Pattern-fitting result of Rietveld refinement with 5K neutron data. In the upper field the points with vertical error bars are the observations and the solid curve is the calculated pattern. The difference is plotted in the lowest field. The short vertical bars in the middle field mark the positions of possible Bragg reflections for the apatite (upper set) and the fluorite (lower set).

Table 2. *Distances and angles*

(*a*) Interatomic distances (Å) in (Ca, Mn) apatite and fluorapatite

Crystal*	Ca(1a^{i})-O(1^{i})	-O(i^{ii})	-O(1^{iii})	-O(2^{iv})	-O(2^{v})	-O(2^{vi})	-O(3b^{i})	-O(3b^{ii})	-O(3b^{iii})
5K	2·35 (1)	2·35 (1)	2·35 (1)	2·40 (1)	2·40 (1)	2·40 (1)	2·843 (8)	2·842 (8)	2·842 (8)
RT	2·36 (1)	2·36 (1)	2·36 (1)	2·38 (1)	2·38 (1)	2·38 (1)	2·866 (8)	2·865 (8)	2·866 (8)
FAp	2·397 (1)	2·397 (1)	2·396 (1)	2·453 (1)	2·452 (1)	2·452 (1)	2·801 (1)	2·800 (1)	2·801 (1)
	Ca(1b^{i})-O(1^{iv})	-O(1^{v})	-O(1^{vi})	-O(2^{i})	-O(2^{ii})	-O(2^{iii})	-O(3a^{i})	-O(3a^{ii})	-O(3a^{iii})
5 K	2·44 (1)	2·44 (1)	2·44 (1)	2·46 (1)	2·46 (1)	2·46 (1)	2·765 (7)	2·765 (7)	2·765 (7)
RT	2·43 (1)	2·43 (1)	2·43 (1)	2·49 (1)	2·49 (1)	2·49 (1)	2·774 (6)	2·773 (6)	2·774 (6)
FAp	2·397 (1)	2·396 (1)	2·397 (1)	2·453 (1)	2·452 (1)	2·452 (1)	2·801 (1)	2·800 (1)	2·801 (1)
	Ca(2^{i})-O(1^{iii})	Ca(2^{i})-O(2^{ii})	Ca(2^{i})-O(3a^{i})	Ca(2^{i})-O(3a^{vi})	Ca(2^{i})-O(3b^{ii})	Ca(2^{i})-O(3b^{iv})	F(1^{i})-Ca(2^{i})	F(1^{i})-Ca(2^{ii})	F(1^{i})-Ca(2^{iii})
5 K	2·687 (2)	2·375 (2)	2·535 (7)	2·301 (8)	2·365 (8)	2·424 (6)	2·292 (2)	2·292 (2)	2·292 (2)
RT	2·692 (3)	2·390 (2)	2·523 (8)	2·330 (9)	2·35 (1)	2·453 (8)	2·292 (2)	2·292 (2)	2·292 (2)
FAp	2·814 (1)	2·384 (1)	2·385 (1)	2·340 (1)	2·398 (1)	2·385 (1)	2·2306 (2)	2·2306 (2)	2·2306 (2)
	P(1^{i})-O(1^{i})	P(1^{i})-O(2^{i})	P(1^{i})-O(3a^{i})	P(1^{i})-O(3b^{iv})					
5 K	1·534 (3)	1·541 (2)	1·480 (9)	1·606 (9)					
RT	1·532 (3)	1·542 (3)	1·49 (1)	1·59 (1)					
FAp	1·534 (1)	1·541 (1)	1·534 (1)	1·534 (1)					

(*b*) Bond angles (°) for the phosphate tetrahedra in the refinement in $P6_3$ for apatite

	O(1)-P(1)-O(2)	O(1)-P(1)-O(3*a*)	O(1)-P(1)-O(3*b*)	O(2)-P(1)-O(3*a*)	O(2)-P(1)-O(3*b*)	O(3*a*)-P(1)-O(3*b*)
5K	111·8 (1)	112·2 (5)	109·7 (5)	111·1 (5)	105·3 (5)	106·4 (3)
RT	111·7 (1)	112·4 (6)	109·4 (6)	111·6 (5)	105·1 (6)	106·2 (4)
FAp	111·29 (5)	111·06 (4)	111·05 (4)	107·95 (4)	107·95 (4)	107·37 (4)

Note: the superscripts in part (*a*) refer to the atom positions in Table 2 translated by the following symmetry operations: (i) x, y, z; (ii) $\bar{y}, x-y, z$; (iii) $y-x, \bar{x}, z$; (iv) $\bar{x}, \bar{y}, \frac{1}{2}+z$; (v) $x-y, x, \frac{1}{2}+z$; (vi) $y, y-x, \frac{1}{2}+z$.

* 5 K and RT refer to the present (Ca, Mn) apatite (RT = room temperature) results in $P6_3$. FAp refers to synthetic fluorapatite (Sudarsanan, Mackie & Young, 1972).

tallized nature of the specimen, the lack of fall-off of the neutron scattering lengths with angle, and the reduction of thermal motion by use of the 5 K temperature have all contributed to the wealth of extractable information in the neutron diffraction pattern.

Interatomic distances and angles calculated with program *ORFFE* (Busing, Martin, Levy, Brown, Johnson & Thiessen, 1979) and the data in Table 1 are listed in Table 2. For comparison purposes, the interatomic distances and angles for single-crystal synthetic fluorapatite, FAp (Sudarsanan, Mackie & Young 1972), have also been calculated and included.

Interpretations and discussion

The most obvious conclusion, evident from the site-occupancy factors in Table 1, is that the Mn substituted essentially only in the Ca(1*a*) subset of the Ca(1) sites (where it suppressed the Ca site-occupancy factor), thus lowering the symmetry from $P6_3/m$ of FAp to $P6_3$. As is discussed in detail later, once a Mn^{2+} ion substitutes at any one Ca(1) site in a cell, it affects the structure in a way that tends to exclude Mn from the other Ca(1) sites.

The site occupancies in Table 1 are scaled relative to $N[O(3a)] = 6{\cdot}00$. But that parameter may also be subject to error, essentially the same fractional error as occurs in the overall scale factor. The average of the site occupancies of the non-Ca atom provides a better reference. Essentially this is the assumption that the non-Ca atoms are, on average, present in stoichiometric amounts. The results of a Rietveld refinement with room-temperature X-ray powder diffraction data were in agreement with this assumption well within the (somewhat larger) e.s.d.'s obtained. Rescaling on that basis led to site occupancies 1·35 (9), 2·09 (9) and 5·77 (18) for Ca(1*a*), Ca(1*b*), and Ca(2), respectively, at 5 K and 1·29 (8), 2·14 (9) and 5·69 (17) at room temperature.

There is no substantial evidence here of Mn substituting for Ca(1*b*), Ca(2) or P. From ESR studies Gilinskaya & Shcherbakova (1971) reported that about 1 in 15 Mn atoms entered the Ca(2) site. With the 5 K site occupancies rescaled as above, one calculates 0·13 (10) Mn per cell possibly present in Ca(2) sites and 0·37 (5) Mn per cell in Ca(1*a*) sites. But, applying the same rule to the Ca(1*b*) site, one calculates −0·05 (5) Mn per cell in those sites, a physical impossibility. Thus, one must simply conclude that the experimental errors here are too large to permit verification or rebuttal of the Gilinskaya & Shcherbakova report. Warren (1970) indicated (his Fig. 7) ~40% of the Mn ions in the Ca(2) site for Mn/Ca ≈ 0·04 in the crystals as it is in the present specimens and a trend toward a higher fraction in the Ca(2) sites with increasing Mn/Ca. Warren & Mazelsky (1974) supported this trend. The present results are probably not in agreement with so much Mn in Ca(2) sites, though the large errors do not permit one to be certain. It should be noted that the Warren (1970) specimens were prepared from the melt differently from ours. With the understanding gained in this work (to be described shortly) of the mechanism of the changes shown in Fig. 1 and considering the Mn/Ca ratio in his charges, LaCout's (1983) results indicate more strongly than do our site-occupancy results that

the Mn in his preparations substituted essentially exclusively at the Ca(1) site.

The non-zero value of the thermal parameters in the apatite phase at 5 K must be interpreted as being due primarily to distortion, essentially random static displacements arising from repositioning of the PO_4 groups adjacent to a Mn^{2+} ion, in the average structure rather than to actual thermal motions. Supporting this interpretation is the fact that the thermal parameters in the fluorite phase at 5 K did refine to values indistinguishable from zero (Table 1).

By reference to the tables and Fig. 3, one sees that Mn at $\frac{2}{3}$, $\frac{1}{3}$, 0·498 attracts the neighboring O(1) at 0·327, 0·485, 0·239 and the O(2) at 0·589, 0·466, 0·254, thus increasing z (above $\frac{1}{4}$) for O(2) and decreasing it for O(1). By the 6_3 symmetry, every O(2) in this Mn-substituted structure must occur above and every O(1) below (in z) the position of the mirror plane at $z=\frac{1}{4}$ (or $\frac{3}{4}$) on which it falls in pure FAp. Looking at the PO_4 tetrahedron just to the left of this Mn site, one sees that these changes in z for O(1) and O(2) tend to tilt the tetrahedron, causing O(3*b*) to move away from the Mn site. That the motion does have a large tilt component is indicated by the large β_{11} for O(3*b*) in the 5 K results (Table 1). It is largely due to the O(3*b*) ions actually being distributed between two positions, one for those O(3*b*) ions which coordinate a Mn^{2+} ion and one for those which do not. Comparison of the various O-to-Ca(1) distances in FAp (Table 2) with those for the present specimen shows that O(3*b*) actually suffers a greater displacement, albeit away from the Mn, by the introduction of Mn than does either O(1) or O(2). Hence it is reasonable that it is O(3*b*) which exhibits the greatest distortion contribution to the apparent thermal factor. The axis of this relative rotation of the phosphate tetrahedron appears to pass essentially through the P position (its $B=0$ Å^2 at 5 K). Clearly it is this rotation which constitutes the structural basis of the 'disturbance of the space homogeneity in the electric crystalline field' reported by Gilinskaya & Shcherbakova (1971) in their EPR study.

It is the interactions with Mn that perturb the phosphate ν_1 vibration from 968 to 959 cm^{-1}. In Fig. 3, one sees that a single Mn atom at, for example, $\frac{2}{3}$, $\frac{1}{3}$, ~0·50 would interact with six different phosphate tetrahedra, which is the total number of phosphate tetrahedra per unit cell. If there were one Mn atom per two unit cells, approximately the situation here, that Mn would interact with one-half of all of the phosphate tetrahedra. Thus, the mechanism is made clear by which the ratio of the absorbance of the Mn-perturbed ν_1 band (959 cm^{-1}) to that of the unperturbed (968 cm^{-1}) should be directly proportional to the fraction of a Mn^{2+} ion per unit cell.

The degree of substitution of Mn^{2+} for $Ca^{2+}(1a)$ in the structure should, therefore, be revealed both by the relative absorbance of the two ν_1 bands and by the suppression of the refined Ca(1*a*) site-occupancy factor. As is reported above, the latter calculation led to ~0·37 (5) Mn atoms per unit cell at the Ca(1*a*) sites. Fig. 4 affords a more quantitative look at the perturbed and unperturbed phosphate ν_1 band intensities than does Fig. 1 for the specimen

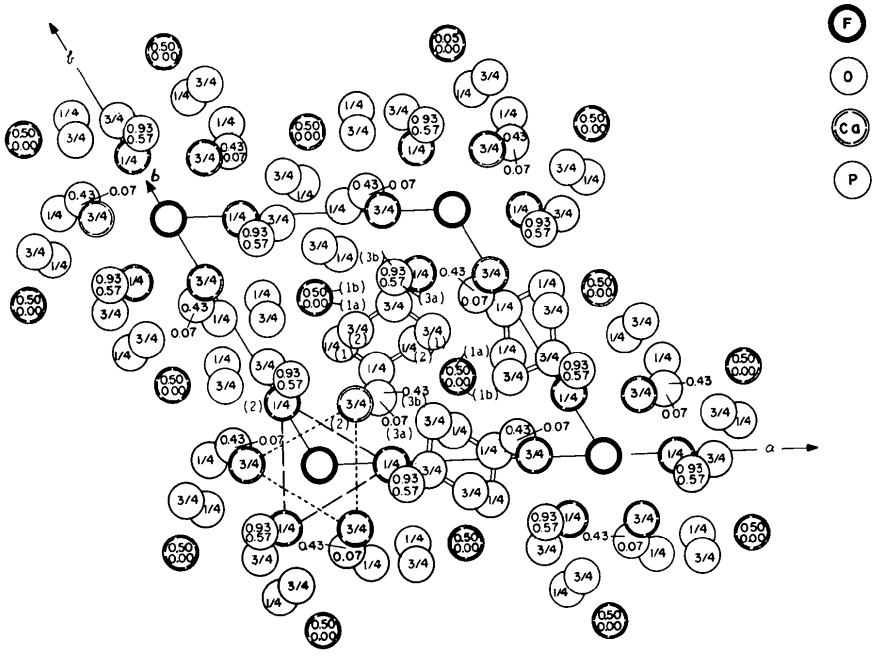

Fig. 3. Fluorapatite structure ($P6_3/m$). The numbers and letters in parentheses designate the subset of the atom type in $P6_3$, the others are z coordinates. F occurs at $z=\frac{1}{4}$ and $\frac{3}{4}$.

studied. The spectra were recorded with a Perkin-Elmer 580B IR spectrometer operating in the linear absorbance mode. It is evident here that the actual area of the unperturbed ν_1 band is greater than that of the Mn-perturbed band, in accord with the structure-refinement result that the Mn content is $\sim\frac{3}{8}$ atom per cell which would, then, perturb only $\sim\frac{3}{8}$ of the phosphate ions. Thus the two degree-of-substitution indicators, relative intensities of the two ν_1 bands and the Ca site-occupancy factor, are in good agreement with each other. The analyzed Mn content (0·448 Mn/cell) is also in acceptable agreement (within 2 e.s.d.) with these results. Any small substitution that might occur at Ca(2) sites would improve this agreement.

Similar reasoning about the Mn-phosphate interaction leads to an understanding of why the structure tends to resist accepting more than one Mn^{2+} ion per cell, as LaCout (1983) noted. One Mn^{2+} ion per cell perturbs all of the phosphate tetrahedra, moving and tilting them in a manner most favorable to itself (*i.e.* minimizing the total free energy). If an additional Mn^{2+} ion were put in at any of the other Ca(1) sites, the effect would be to tend to tilt the neighboring phosphate tetrahedra oppositely from the way they are tilted by the one Mn per cell. The result would be that all Mn–O(1) and Mn–O(2) bonds would be lengthened and, apparently, the lattice free energy would be higher than it would be without the Mn^{2+} ion, or ions, in excess of one per cell. This mechanism of preference for only one Mn^{2+} ion per cell also leads to the prediction that in $Ca_9Mn_1(PO_4)_6F_2$ the Mn^{2+} ions should occur in an ordered subset of one-fourth of the Ca(1) sites.

An attempt was made to address the question of whether the Mn may actually order further, in a subset of the Ca(1*a*) sites: refinements were carried out in *P*3. Individual isotropic thermal parameters were used. Because there were so many refined parameters (94), the standard deviations were much larger for the refinements in *P*3 and the results are therefore not presented as being meaningful in detail. However, the various Ca(1)–O distances calculated from the refined positional parameters were reasonably consistent with the thermal parameters treated two different ways (Table 3). By indicating which phosphate tetrahedron is most rotated [*via* shorter distances from the Mn-occupied Ca(1) site to O(1) and O(2) and increased distances to O(3)] they suggest that the Mn may, in fact, tend to substitute in a subset of the Ca(1*a*) sites, that at $\frac{1}{3}$, $\frac{2}{3}$, 0·0 in each cell. Thus, the somewhat inconclusive refinements in *P*3 suggest that the ordering in a subset of Ca(1*a*) expected with one Mn^{2+} per unit cell may have already started with the approximately $\frac{3}{8}$ Mn present here.

Table 3. *Some results from refinements in P*3

Present specimen				
		Distance (Å)		
Ca(1)	O	with *B*'s fixed*	with overall *B*†	Distance in FAp (Å)
a	3*c*	2·93 (1)	2·92 (2)	2·801 (1)
a	1*a*	2·33 (3)	2·37 (3)	2·396 (1)
a	2*b*	2·45 (3)	2·44 (3)	2·453 (1)
b	3*b*	2·74 (1)	2·82 (2)	2·80
b	1*a*	2·45 (3)	2·44 (3)	2·40
b	2*b*	2·43 (3)	2·41 (3)	2·45
c	3*a*	2·77 (2)	2·67 (2)	2·80
c	1*b*	2·44 (3)	2·39 (3)	2·40
c	2*a*	2·49 (3)	2·54 (3)	2·45
d	3*d*	2·77 (1)	2·79 (2)	2·80
d	1*b*	2·34 (3)	2·36 (3)	2·40
d	2*a*	2·36 (3)	2·35 (3)	2·45

Designation of Ca(1) sites in *P*3				
Site	*x*	*y*	*z*	
		fixed*	with *B*'s *B*†	with overall
Ca 1*a*	$\frac{1}{3}$	$\frac{2}{3}$	0·009 (5)	0·002 ( )
1*b*	$\frac{1}{3}$	$\frac{2}{3}$	0·504 (6)	0·506 (4)
1*c*	$\frac{2}{3}$	$\frac{1}{3}$	0·003 (4)	−0·005 (4)
1*d*	$\frac{2}{3}$	$\frac{1}{3}$	0·500 (6)	0·502 (6)

* Individual *B*'s were fixed at values resulting from their refinement simultaneously with the positional parameters and site occupancies, in $P6_3$.
† Individual *B*'s were fixed at 0 Å^2 and only a single overall *B* was varied simultaneously with the positional parameters and site occupancies.

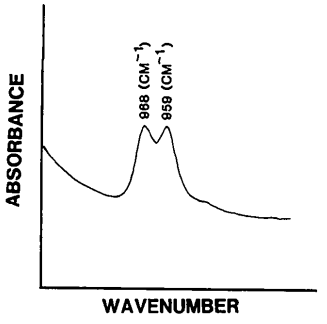

Fig. 4. The Mn-perturbed (959 cm^{-1}) and the unperturbed ν_1 IR bands for the PO_4 groups in the specimen studied.

Technical assistance of D. W. Holcomb, particularly with the IR work for Fig. 4, and very useful comments of Dr B. DeBoer on an earlier draft are gratefully acknowledged. This work was supported in part by the USPHS through NIH-NIDR Grant DE-01912.

References

BARATALI, T., HEUGHEBAERT, J. C., SERIOT, J. & MONTEL, G. (1976). *C.R. Acad. Sci. Sér. C*, **282**, 31.

BUSING, W. R., MARTIN, K. O., LEVY, H. A., BROWN, G. M., JOHNSON, C. K. & THIESSEN, W. E. (1979). Updated version of *ORFFE*4: accession No. 85, *World List of Crystallographic Computer Programs*, 3rd ed. [*J. Appl. Cryst.* (1973), **6**, 309-346].

CURZON, M. E. J. & CROCKER, D. C. (1978). *Arch. Oral Biol.* **23**, 647-653.

GILINSKAYA, L. G. & SHCHERBAKOVA, M. JA. (1971). Proc. XVIth Congr. Ampere, Bucharest.

HEUGHEBAERT, J. C., SERIOT, J., JOUKOFF, B., GAUMEMAHN, F. & MONTEL, G. (1975). *C.R. Acad. Sci. Sér. C*, **281**, 615.
JOHNSON, P. D. (1962). *Luminescence of Organic and Inorganic Materials*, p. 563. New York: John Wiley.
KASAI, P. (1962). *J. Phys. Chem.* **66**, 671-680.
KINGSLEY, J. D., PRENER, J. S. & SEGALL, B. (1965). *Phys. Rev. A*, **137**, 189-202.
LACOUT, J. L. (1983). Thèse, Institut National Polytechnique, Toulouse.
OHKUBO, Y. (1969). *J. Phys. Soc. Jpn*, **27**, 1516-1526.
SUDARSANAN, K., MACKIE, P. E. & YOUNG, R. A. (1972). *Mater. Res. Bull.* **7**, 1331-1338.
SWANSON, H. E. & TATGE, E. (1951). *Natl Bur. Stand. (US) Circ.* No. 539, p. 70.
WARREN, R. W. (1970). *Phys. Rev. B*, **2**, 4383-4388.
WARREN, R. W. & MAZELSKY, R. (1974). *Phys. Rev. B*, **10**, 19-25.
WILES, D. B. & YOUNG, R. A. (1981). *J. Appl. Cryst.* **14**, 149-151.

Acta Cryst. (1985). B**41**, 179-184

High-Pressure Behavior of $LaNbO_4$

BY J. W. E. MARIATHASAN*

Clarendon Laboratory, Parks Road, Oxford OX1 3PU, England

AND L. W. FINGER AND R. M. HAZEN

Geophysical Laboratory, Carnegie Institution of Washington, Washington DC 20008, *USA*

(*Received* 30 *July* 1984; *accepted* 7 *November* 1984)

Abstract

Unit-cell and crystal structure parameters of $LaNbO_4$ with a distorted scheelite structure have been refined at room pressure (489 reflections; weighted $R = 0{\cdot}021$), at 1·55 GPa (207 reflections; weighted $R = 0{\cdot}034$), and at 3·26 GPa (201 reflections; weighted $R = 0{\cdot}034$). Compression is very anisotropic with maximum compressibility [0·07(1) GPa^{-1}] near the (310) plane but expansion with increasing pressure [−0·010(3) GPa^{-1}] approximately parallel to the [310] direction. The bulk modulus of $LaNbO_4$ (with $K' = 4$) is 0·111(3) TPa. The high-pressure structural behavior of $LaNbO_4$, in which the monoclinic distortion increases with increasing pressure, is opposite to that of isostructural $BiVO_4$. This behavior is related to structural instabilities that result in ferroelastic transitions in scheelite-type compounds. A value of 3·83 K/0·1 GPa is calculated for dT_c/dP. The high-pressure structure is analyzed in terms of bond-length–bond-strength concepts and the 'inverse' relationships of temperature and pressure.

Introduction

Ferroelastic properties of compounds with distorted scheelite structures, including $BiVO_4$ and the rare-earth niobates, have been of recent interest. Measurements of high-pressure Raman scattering, birefringence, and X-ray scattering have been made by Pinczuk, Welber & Dacol (1979), Wood, Welber, David & Glazer (1980), and Hazen & Mariathasan (1982), respectively. The present study reports the high-pressure behavior of $LaNbO_4$, which has a ferroelastic transition at high temperature similar to that of $BiVO_4$. Lattice constants and structural parameters have been determined at pressures up to 3·26 GPa, and the variation of the transformation temperature with pressure has been estimated.

Understanding of the structure of rare-earth niobates has been confused since Barth (1926) first examined the mineral fergusonite, Y(Nb, Ta)O_4, and concluded that it was tetragonal, isostructural with scheelite. Ferguson (1957) found that synthetic crystals of $YTaO_4$ were monoclinic rather than tetragonal. This discrepancy was resolved by Komkov (1959), who showed that naturally occurring fergusonite could be transformed from a (metastable) scheelite structure to a stable monoclinic form by annealing. Komkov used Patterson syntheses to conclude that the space group must be $I2$ (C_2^3) rather than $I2/a$ (C_{2h}^6) or Ia (C_s^4), even though all three satisfy the systematic absences. Brixner, Whitney, Zumsteg & Jones (1977) used a Czochralski-pulled crystal to examine the domain structure of $LaNbO_4$, observed only two types of domain walls, and concluded that the correct low-temperature space group had half the number of symmetry elements of the high-temperature group, $I4_1/a$ (C_{4h}^6). This conclusion implied a low-temperature symmetry of $I2/a$ (C_{2h}^6).

Although the three possible space groups have identical systematic absences, they belong to different point groups and have different symmetry in conver-

* Present address: Smith Associates, 45-47 High Street, Cobham, Surrey KT11 3DP, England.

0108-7681/85/030179-06$01.50